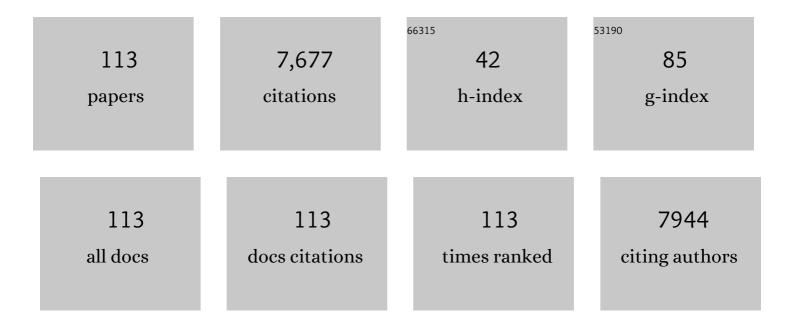
List of Publications by Year in descending order

Source: https://exaly.com/author-pdf/4534682/publications.pdf Version: 2024-02-01



#	Article	IF	CITATIONS
1	Magnetic resonance tracking of dendritic cells in melanoma patients for monitoring of cellular therapy. Nature Biotechnology, 2005, 23, 1407-1413.	9.4	791
2	Prostate Cancer: Multiparametric MR Imaging for Detection, Localization, and Staging. Radiology, 2011, 261, 46-66.	3.6	618
3	Clinical Proton MR Spectroscopy in Central Nervous System Disorders. Radiology, 2014, 270, 658-679.	3.6	524
4	Prostate Cancer Localization with Dynamic Contrast-enhanced MR Imaging and Proton MR Spectroscopic Imaging. Radiology, 2006, 241, 449-458.	3.6	506
5	Prostate Cancer: Body-Array versus Endorectal Coil MR Imaging at 3 T—Comparison of Image Quality, Localization, and Staging Performance. Radiology, 2007, 244, 184-195.	3.6	295
6	Methodological consensus on clinical proton MRS of the brain: Review and recommendations. Magnetic Resonance in Medicine, 2019, 82, 527-550.	1.9	280
7	Prospective Assessment of Prostate Cancer Aggressiveness Using 3-T Diffusion-Weighted Magnetic Resonance Imaging–Guided Biopsies Versus a Systematic 10-Core Transrectal Ultrasound Prostate Biopsy Cohort. European Urology, 2012, 61, 177-184.	0.9	277
8	Short echo time <sup>1</sup> Hâ€MRSI of the human brain at 3T with minimal chemical shift displacement errors using adiabatic refocusing pulses. Magnetic Resonance in Medicine, 2008, 59, 1-6.	1.9	257
9	IMRT boost dose planning on dominant intraprostatic lesions: Gold marker-based three-dimensional fusion of CT with dynamic contrast-enhanced and 1H-spectroscopic MRI. International Journal of Radiation Oncology Biology Physics, 2006, 65, 291-303.	0.4	168
10	Prostate Cancer: Local Staging at 3-T Endorectal MR Imaging—Early Experience. Radiology, 2006, 238, 184-191.	3.6	159
11	Assessment of Prostate Cancer Aggressiveness Using Dynamic Contrast-enhanced Magnetic Resonance Imaging at 3 T. European Urology, 2013, 64, 448-455.	0.9	152
12	Initial Experience of 3 Tesla Endorectal Coil Magnetic Resonance Imaging and 1H-Spectroscopic Imaging of the Prostate. Investigative Radiology, 2004, 39, 671-680.	3.5	148
13	Towards 1H-MRSI of the human brain at 7T with slice-selective adiabatic refocusing pulses. Magnetic Resonance Materials in Physics, Biology, and Medicine, 2008, 21, 95-101.	1.1	135
14	Prostate Cancer Aggressiveness: In Vivo Assessment of MR Spectroscopy and Diffusion-weighted Imaging at 3 T. Radiology, 2012, 265, 457-467.	3.6	127
15	Three-dimensional Proton MR Spectroscopy of Human Prostate at 3 T without Endorectal Coil: Feasibility. Radiology, 2007, 245, 507-516.	3.6	122
16	Quantitative MR imaging of individual muscle involvement in facioscapulohumeral muscular dystrophy. Neuromuscular Disorders, 2009, 19, 357-362.	0.3	120
17	Electroosmotic and Pressure-Driven Flow in Open and Packed Capillaries:  Velocity Distributions and Fluid Dispersion. Analytical Chemistry, 2000, 72, 2292-2301.	3.2	118
18	Fast acquisition-weighted three-dimensional proton MR spectroscopic imaging of the human prostate. Magnetic Resonance in Medicine, 2004, 52, 80-88.	1.9	108

#	Article	IF	CITATIONS
19	Advanced single voxel <sup>1</sup> H magnetic resonance spectroscopy techniques in humans: Experts' consensus recommendations. NMR in Biomedicine, 2021, 34, e4236.	1.6	98
20	Optimal timing for in vivo1H-MR spectroscopic imaging of the human prostate at 3T. Magnetic Resonance in Medicine, 2005, 53, 1268-1274.	1.9	91
21	In Vivo Assessment of Prostate Cancer Aggressiveness Using Magnetic Resonance Spectroscopic Imaging at 3 T with an Endorectal Coil. European Urology, 2011, 60, 1074-1080.	0.9	91
22	Quantitative Evaluation of Computed High b Value Diffusion-Weighted Magnetic Resonance Imaging of the Prostate. Investigative Radiology, 2013, 48, 779-786.	3.5	86
23	Sensitivity of magnetic resonance imaging of dendritic cells for in vivo tracking of cellular cancer vaccines. International Journal of Cancer, 2006, 120, 978-984.	2.3	82
24	MRI of intact plants. Photosynthesis Research, 2009, 102, 213-222.	1.6	81
25	Prostate MRI and 3D MR Spectroscopy: How We Do It. American Journal of Roentgenology, 2010, 194, 1414-1426.	1.0	80
26	Feasibility of a Pneumatically Actuated MR-compatible Robot for Transrectal Prostate Biopsy Guidance. Radiology, 2011, 260, 241-247.	3.6	80
27	Multiparametric Magnetic Resonance Imaging in Prostate Cancer Management. Investigative Radiology, 2015, 50, 594-600.	3.5	78
28	Standardized Threshold Approach Using Three-Dimensional Proton Magnetic Resonance Spectroscopic Imaging in Prostate Cancer Localization of the Entire Prostate. Investigative Radiology, 2007, 42, 116-122.	3.5	70
29	Ultraâ€small superparamagnetic iron oxides for metastatic lymph node detection: back on the block. Wiley Interdisciplinary Reviews: Nanomedicine and Nanobiotechnology, 2018, 10, e1471.	3.3	70
30	Prostate Cancer Evaluated with Ferumoxtran-10–enhanced T2*-weighted MR Imaging at 1.5 and 3.0 T: Early Experience. Radiology, 2006, 239, 481-487.	3.6	67
31	Discriminating Cancer From Noncancer Tissue in the Prostate by 3-Dimensional Proton Magnetic Resonance Spectroscopic Imaging. Investigative Radiology, 2011, 46, 25-33.	3.5	67
32	Multiparametric Magnetic Resonance Imaging for Discriminating Low-Grade From High-Grade Prostate Cancer. Investigative Radiology, 2015, 50, 490-497.	3.5	63
33	Evaluation of a robotic technique for transrectal MRI-guided prostate biopsies. European Radiology, 2012, 22, 476-483.	2.3	60
34	Prostate Cancer: Precision of Integrating Functional MR Imaging with Radiation Therapy Treatment by Using Fiducial Gold Markers. Radiology, 2005, 236, 311-317.	3.6	58
35	Comparing localized and nonlocalized dynamic <sup>31</sup> P magnetic resonance spectroscopy in exercising muscle at 7T. Magnetic Resonance in Medicine, 2012, 68, 1713-1723.	1.9	55
36	Functional Imaging of Plants: A Nuclear Magnetic Resonance Study of a Cucumber Plant. Biophysical Journal, 2002, 82, 481-492.	0.2	53

#	Article	IF	CITATIONS
37	Lutetium-177-PSMA-617 in Low-Volume Hormone-Sensitive Metastatic Prostate Cancer: A Prospective Pilot Study. Clinical Cancer Research, 2021, 27, 3595-3601.	3.2	53
38	Changes in Prostate Shape and Volume and Their Implications for Radiotherapy After Introduction of Endorectal Balloon as Determined by MRI at 3T. International Journal of Radiation Oncology Biology Physics, 2009, 73, 1446-1453.	0.4	52
39	Dynamic NMR microscopy of chromatographic columns. AICHE Journal, 1998, 44, 1962-1975.	1.8	47
40	In vivo 13C magnetic resonance spectroscopy of a human brain tumor after application of 13C-1-enriched glucose. Magnetic Resonance Imaging, 2010, 28, 690-697.	1.0	47
41	GABAergic changes in the thalamocortical circuit in Parkinson's disease. Human Brain Mapping, 2020, 41, 1017-1029.	1.9	46
42	Short echo time <sup>1</sup> H MRSI of the human brain at 3T with adiabatic sliceâ€selective refocusing pulses; reproducibility and variance in a dual center setting. Journal of Magnetic Resonance Imaging, 2010, 31, 61-70.	1.9	45
43	The accuracy and safety aspects of a novel robotic needle guide manipulator to perform transrectal prostate biopsies. Medical Physics, 2010, 37, 4744-4750.	1.6	43
44	Semi-LASER localized dynamic <sup>31</sup> P magnetic resonance spectroscopy in exercising muscle at ultra-high magnetic field. Magnetic Resonance in Medicine, 2011, 65, 1207-1215.	1.9	39
45	Feasibility of <i>T</i> <sub>2</sub> -weighted turbo spin echo imaging of the human prostate at 7 tesla. Magnetic Resonance in Medicine, 2014, 71, 1711-1719.	1.9	36
46	Macroscopic Heterogeneities in Electroosmotic and Pressure-Driven Flow through Fixed Beds at Low Column-to-Particle Diameter Ratio. Journal of Physical Chemistry B, 2001, 105, 8591-8599.	1.2	34
47	Quantitative19F MR spectroscopy at 3 T to detect heterogeneous capecitabine metabolism in human liver. NMR in Biomedicine, 2007, 20, 485-492.	1.6	34
48	In vivo <sup>31</sup> P MR spectroscopic imaging of the human prostate at 7 T: Safety and feasibility. Magnetic Resonance in Medicine, 2012, 68, 1683-1695.	1.9	34
49	In vivo clearance of 19F MRI imaging nanocarriers is strongly influenced by nanoparticle ultrastructure. Biomaterials, 2020, 261, 120307.	5.7	33
50	Metabolite ratios in <sup>1</sup> H MR spectroscopic imaging of the prostate. Magnetic Resonance in Medicine, 2015, 73, 1-12.	1.9	32
51	7T ultraâ€high field body <scp>MR</scp> imaging with an 8â€channel transmit/32â€channel receive radiofrequency coil array. Medical Physics, 2018, 45, 2978-2990.	1.6	32
52	Lutetium-177-PSMA-I&T as metastases directed therapy in oligometastatic hormone sensitive prostate cancer, a randomized controlled trial. BMC Cancer, 2020, 20, 884.	1.1	32
53	<sup>1</sup> H–MRS processing parameters affect metabolite quantification: The urgent need for uniform and transparent standardization. NMR in Biomedicine, 2017, 30, e3804.	1.6	31
54	Oligometastatic Prostate Cancer: Results of a Dutch Multidisciplinary Consensus Meeting. European Urology Oncology, 2020, 3, 231-238.	2.6	30

#	Article	IF	CITATIONS
55	Mapping of prostate cancer by <sup>1</sup> H MRSI. NMR in Biomedicine, 2014, 27, 39-52.	1.6	29
56	Contribution of Histopathologic Tissue Composition to Quantitative MR Spectroscopy and Diffusion-weighted Imaging of the Prostate. Radiology, 2016, 278, 801-811.	3.6	29
57	<sup>31</sup> P MR spectroscopic imaging of the human prostate at 7 T: T <sub>1</sub> relaxation times, Nuclear Overhauser Effect, and spectral characterization. Magnetic Resonance in Medicine, 2015, 73, 909-920.	1.9	27
58	InÂvivo MR spectroscopic imaging of the prostate, from application to interpretation. Analytical Biochemistry, 2017, 529, 158-170.	1.1	26
59	Head-to-Head Comparison of <sup>68</sup> Ga-Prostate-Specific Membrane Antigen PET/CT and Ferumoxtran-10–Enhanced MRI for the Diagnosis of Lymph Node Metastases in Prostate Cancer Patients. Journal of Nuclear Medicine, 2021, 62, 1258-1263.	2.8	26
60	Prostate and Lymph Node Proton Magnetic Resonance (MR) Spectroscopic Imaging with External Array Coils at 3 T to Detect Recurrent Prostate Cancer After Radiation Therapy. Investigative Radiology, 2007, 42, 420-427.	3.5	25
61	A Single-Arm, Multicenter Validation Study of Prostate Cancer Localization and Aggressiveness With a Quantitative Multiparametric Magnetic Resonance Imaging Approach. Investigative Radiology, 2019, 54, 437-447.	3.5	24
62	Improved volume selective <sup>1</sup> H MR spectroscopic imaging of the prostate with gradient offset independent adiabaticity pulses at 3 tesla. Magnetic Resonance in Medicine, 2015, 74, 915-924.	1.9	23
63	<i>T</i> 1â€weighted MR image contrast around a cryoablation iceball: A phantom study and initial comparison with <i>in vivo</i> findings. Medical Physics, 2014, 41, 112301.	1.6	22
64	Initial Results of 3-Dimensional 1H-Magnetic Resonance Spectroscopic Imaging in the Localization of Prostate Cancer at 3 Tesla. Investigative Radiology, 2011, 46, 301-306.	3.5	21
65	In vivo <sup>1</sup> <scp>H</scp> <scp>MR</scp> spectroscopic imaging of aggressive prostate cancer: Can we detect lactate?. Magnetic Resonance in Medicine, 2014, 71, 26-34.	1.9	21
66	Phosphorus Magnetic Resonance Spectroscopic Imaging at 7 T in Patients With Prostate Cancer. Investigative Radiology, 2014, 49, 363-372.	3.5	20
67	Optimized 31 P MRS in the human brain at 7 T with a dedicated RF coil setup. NMR in Biomedicine, 2015, 28, 1570-1578.	1.6	20
68	Multi-component quantitative magnetic resonance imaging by phasor representation. Scientific Reports, 2017, 7, 861.	1.6	20
69	Metabolic imaging of multiple Xâ€nucleus resonances. Magnetic Resonance in Medicine, 2013, 70, 169-175.	1.9	19
70	3D <sup>31</sup> P MR spectroscopic imaging of the human brain at 3 T with a <sup>31</sup> P receive array: An assessment of <sup>1</sup> H decoupling, T <sub>1</sub> relaxation times, <sup>1</sup> Hâ€ <sup>31</sup> P nuclear Overhauser effects and NAD <sup>+</sup> . NMR in Biomedicine, 2021, 34, e4169.	1.6	18
71	USPIO-enhanced MRI of pelvic lymph nodes at 7-T: preliminary experience. European Radiology, 2019, 29, 6529-6538.	2.3	17
72	The Role of Magnetic Resonance Imaging in (Future) Cancer Staging. Investigative Radiology, 2021, 56, 42-49.	3.5	17

#	Article	IF	CITATIONS
73	Repeatability of <sup>31</sup> P MRSI in the human brain at 7 T with and without the nuclear Overhauser effect. NMR in Biomedicine, 2016, 29, 256-263.	1.6	16
74	1 H MR spectroscopic imaging of the prostate at 7 T using spectralâ€spatial pulses. Magnetic Resonance in Medicine, 2016, 75, 933-945.	1.9	16
75	High resolution <scp>MR</scp> imaging of pelvic lymph nodes at 7 Tesla. Magnetic Resonance in Medicine, 2017, 78, 1020-1028.	1.9	16
76	Reproducibility of 3D <sup>1</sup> H MR spectroscopic imaging of the prostate at 1.5T. Journal of Magnetic Resonance Imaging, 2012, 35, 166-173.	1.9	15
77	Quality control of prostate <sup>1</sup> H MRSI data. NMR in Biomedicine, 2013, 26, 193-203.	1.6	15
78	Role of highâ€field MR in studies of localized prostate cancer. NMR in Biomedicine, 2014, 27, 67-79.	1.6	15
79	Direct dynamic measurement of intracellular and extracellular lactate in smallâ€volume cell suspensions with <sup>13</sup> C hyperpolarised NMR. NMR in Biomedicine, 2015, 28, 1040-1048.	1.6	14
80	High field imaging of large-scale neurotransmitter networks: Proof of concept and initial application to epilepsy. NeuroImage: Clinical, 2018, 19, 47-55.	1.4	13
81	The influence of endorectal filling on rectal cancer staging with MRI. British Journal of Radiology, 2018, 91, 20180205.	1.0	13
82	Update to a randomized controlled trial of lutetium-177-PSMA in Oligo-metastatic hormone-sensitive prostate cancer: the BULLSEYE trial. Trials, 2021, 22, 768.	0.7	13
83	USPIO-enhanced MRI of lymph nodes in rectal cancer: A node-to-node comparison with histopathology. European Journal of Radiology, 2021, 138, 109636.	1.2	12
84	Spatially resolved transport properties in radially compressed bead packings studied by PFG NMR. Magnetic Resonance Imaging, 1998, 16, 703-706.	1.0	11
85	Using NMR displacement imaging to characterize electroosmotic flow in porous media. Magnetic Resonance Imaging, 2001, 19, 453-456.	1.0	11
86	3D MR thermometry of frozen tissue: Feasibility and accuracy during cryoablation at 3T. Journal of Magnetic Resonance Imaging, 2016, 44, 1572-1579.	1.9	11
87	Feasibility of Multiparametric Magnetic Resonance Imaging of the Prostate at 7 T. Investigative Radiology, 2017, 52, 295-301.	3.5	10
88	Imaging Hyperpolarized Pyruvate and Lactate after Blood–Brain Barrier Disruption with Focused Ultrasound. ACS Chemical Neuroscience, 2019, 10, 2591-2601.	1.7	10
89	Is visual activation associated with changes in cerebral high-energy phosphate levels?. Brain Structure and Function, 2018, 223, 2721-2731.	1.2	9
90	An 8â€channel receive array for improved <sup>31</sup> P MRSI of the whole brain at 3T. Magnetic Resonance in Medicine, 2019, 82, 825-832.	1.9	9

#	Article	IF	CITATIONS
91	Controlled mechanical ventilation to detect regional lymph node metastases in esophageal cancer using USPIO-enhanced MRI; comparison of image quality. Magnetic Resonance Imaging, 2020, 74, 258-265.	1.0	9
92	Flexible proton 3 <scp>D</scp> <scp>MR</scp> spectroscopic imaging of the prostate with lowâ€power adiabatic pulses for volume selection and spiral readout. Magnetic Resonance in Medicine, 2017, 77, 928-935.	1.9	8
93	Can Ex Vivo Magnetic Resonance Imaging of Rectal Cancer Specimens Improve the Mesorectal Lymph Node Yield for Pathological Examination?. Investigative Radiology, 2019, 54, 645-652.	3.5	7
94	Reducing Acquisition Time of Diffusion Weighted MR Imaging of the Rectum with Simultaneous Multi-Slice Acquisition: A Reader Study. Academic Radiology, 2022, 29, 1802-1807.	1.3	7
95	A multitransmit external body array combined with a <sup>1</sup> H and <sup>31</sup> P endorectal coil to enable a multiparametric and multimetabolic MRI examination of the prostate at 7T. Medical Physics, 2019, 46, 3893-3905.	1.6	6
96	Novel Diagnostic Approaches for Assessment of the Clinically Negative Neck in Head and Neck Cancer Patients. Frontiers in Oncology, 2020, 10, 637513.	1.3	6
97	Developments in proton MR spectroscopic imaging of prostate cancer. Magnetic Resonance Materials in Physics, Biology, and Medicine, 2022, 35, 645-665.	1.1	6
98	Ultra-high-field MR in Prostate cancer: Feasibility and Potential. Magnetic Resonance Materials in Physics, Biology, and Medicine, 2022, 35, 631-644.	1.1	6
99	High-Accuracy Nodal Staging of Head and Neck Cancer With USPIO-Enhanced MRI. Investigative Radiology, 2022, 57, 810-818.	3.5	6
100	Three-dimensional proton magnetic resonance spectroscopic imaging with and without an endorectal coil: a prostate phantom study. Acta Radiologica, 2015, 56, 1342-1349.	0.5	5
101	Simple and broadly applicable automatic quality control for 3D <sup>1</sup> H MR spectroscopic imaging data of the prostate. Magnetic Resonance in Medicine, 2019, 81, 2887-2895.	1.9	5
102	Pyruvateâ€lactate exchange and glucose uptake in human prostate cancer cell models. A study in xenografts and suspensions by hyperpolarized [1â€13C]pyruvate MRS and [18F]FDGâ€PET. NMR in Biomedicine, 2020, 33, e4362.	1.6	5
103	Magnetic resonance imaging at ultra-high magnetic field strength: An in vivo assessment of number, size and distribution of pelvic lymph nodes. PLoS ONE, 2020, 15, e0236884.	1.1	5
104	Dynamic Nuclear Polarization of Silicon Carbide Micro- and Nanoparticles. ACS Applied Materials & amp; Interfaces, 2021, 13, 30835-30843.	4.0	5
105	Clinical Comparison Between a Currently Available Single-Loop and an Investigational Dual-Channel Endorectal Receive Coil for Prostate Magnetic Resonance Imaging. Investigative Radiology, 2014, 49, 15-22.	3.5	4
106	Simultaneous 18F-fluciclovine Positron Emission Tomography and Magnetic Resonance Spectroscopic Imaging of Prostate Cancer. Frontiers in Oncology, 2018, 8, 516.	1.3	4
107	Prior PSMA PET-CT Imaging and Hounsfield Unit Impact on Tumor Yield and Success of Molecular Analyses from Bone Biopsies in Metastatic Prostate Cancer. Cancers, 2020, 12, 3756.	1.7	4
108	In Vivo PET Imaging of Monocytes Labeled with [89Zr]Zr-PLGA-NH2 Nanoparticles in Tumor and Staphylococcus aureus Infection Models. Cancers, 2021, 13, 5069.	1.7	4

#	Article	IF	CITATIONS
109	A Comprehensive Grading System for a Magnetic Sentinel Lymph Node Biopsy Procedure in Head and Neck Cancer Patients. Cancers, 2022, 14, 678.	1.7	3
110	19F MRI Imaging Strategies to Reduce Isoflurane Artifacts in In Vivo Images. Molecular Imaging and Biology, 2022, 24, 71-81.	1.3	2
111	Validation of In Vivo Nodal Assessment of Solid Malignancies with USPIO-Enhanced MRI: A Workflow Protocol. Methods and Protocols, 2022, 5, 24.	0.9	2
112	PS02.078: FEASIBILITY OF PREOPERATIVE STAGING WITH USPIO ENHANCED MRI IN PATIENTS WITH RESECTABLE ESOPHAGEAL CARCINOMA (PRECIES STUDY). Ecological Management and Restoration, 2018, 31, 142-142.	0.2	0
113	Dualâ€purpose coils in MRSI of brain tumours. NMR in Biomedicine, 2022, 35, e4660.	1.6	0